

# Phonon Confinement Effect in Two-dimensional Nanocrystallites of Monolayer MoS<sub>2</sub> to Probe Phonon Dispersion Trends Away from Brillouin-Zone Center \*

Wei Shi(石薇), Xin Zhang(张昕), Xiao-Li Li(李晓莉), Xiao-Fen Qiao(乔晓粉), Jiang-Bin Wu(吴江滨), Jun Zhang(张俊), Ping-Heng Tan(谭平恒)\*\*

State Key Laboratory of Superlattices and Microstructures, Institute of Semiconductors, Chinese Academy of Sciences, Beijing 100083

(Received 3 March 2016)

The fundamental momentum conservation requirement  $q \sim 0$  for the Raman process is relaxed in the nanocrystallites (NCs), and phonons away from the Brillouin-zone center will be involved in the Raman scattering, which is well-known as the phonon confinement effect in NCs. This usually gives a downshift and asymmetric broadening of the Raman peak in various NCs. Recently, the  $A'_1$  mode of 1L MoS<sub>2</sub> NCs is found to exhibit a blue shift and asymmetric broadening toward the high-frequency side [Chem. Soc. Rev. 44 (2015) 2757 and Phys. Rev. B 91 (2015) 195411]. In this work, we carefully check this issue by studying Raman spectra of 1L MoS<sub>2</sub> NCs prepared by the ion implantation technique in a wide range of ion-implanted dosage. The same confinement coefficient is used for both  $E'$  and  $A'_1$  modes in 1L MoS<sub>2</sub> NCs since the phonon uncertainty in an NC is mainly determined by its domain size. The asymmetrical broadening near the  $A'_1$  and  $E'$  modes is attributed to the appearance of defect-activated phonons at the zone edge and the intrinsic asymmetrical broadening of the two modes, where the anisotropy of phonon dispersion curves along  $\Gamma$ - $K$  and  $\Gamma$ - $M$  is also considered. The photoluminescence spectra confirm the formation of small domain size of 1L MoS<sub>2</sub> nanocrystallites in the ion-implanted 1L MoS<sub>2</sub>. This study provides not only an approach to quickly probe phonon dispersion trends of 2D materials away from  $\Gamma$  by the Raman scattering of the corresponding NCs, but also a reference to completely understand the confinement effect of different modes in various nanomaterials.

PACS: 78.30.Ly, 61.72.U- , 63.20.D-

DOI: 10.1088/0256-307X/33/5/057801

With the advent of the exfoliation technique for preparing atomically thin sheets,<sup>[1]</sup> layered materials (LMs) spark wide interest over the world. Among LMs, transition-metal dichalcogenides (TMDs) MX<sub>2</sub> have been widely studied due to their distinctive electronic and optical properties.<sup>[2,3]</sup> MoS<sub>2</sub> is a typical TMD. Its band gap exhibits an indirect-to-direct transition from a few layers to monolayer (1L),<sup>[4]</sup> enabling many applications in electronics and optoelectronics.<sup>[2]</sup> Optical or electronic excitations can be scattered by phonons into different states or can decay into vibrational excitations, therefore, phonons also play an important role in electrical transport properties and excited-state dynamics.<sup>[5]</sup> Indeed, the carrier mobility in monolayer MoS<sub>2</sub> is mainly limited by optical phonon scattering due to deformation potential and the Fröhlich interactions,<sup>[6]</sup> and phonons near the  $K$  points of the Brillouin-zone (BZ) can directly affect valley polarization due to the momentum change of inter-valley scattering.<sup>[7]</sup> Probing phonons at  $\Gamma$  and its energy dispersion in the BZ of solids is thus of primary importance for fundamental science and applications.

Raman scattering is mainly applied to detect phonons at  $\Gamma$ . Due to the Heisenberg uncertainty principle, the fundamental  $q \sim 0$  Raman selection rule is relaxed for nanocrystallites (NCs) with a finite do-

main size ( $L_D$ ), which make phonon uncertainty of  $\Delta q \sim 1/L_D$  be involved in the Raman scattering.<sup>[8]</sup> This allows participation of phonons away from the BZ center ( $\Gamma$ ), which usually gives a downshift and asymmetric broadening of the Raman peak for various NCs.<sup>[8-14]</sup> It becomes a common concept that the Raman peaks in NCs will exhibit a redshift in frequency with decreasing  $L_D$ . However, the  $A'_1$  mode of 1L MoS<sub>2</sub> NCs is recently found to exhibit unusual behavior with respect to the common Si, Ge and GaAs nanocrystallites, exhibiting a blueshift in frequency and asymmetric broadening toward the high frequency side.<sup>[15,16]</sup> It is noteworthy that the physical origins of phonon confinement effect for the  $A'_1$  and  $E'$  modes in monolayer MoS<sub>2</sub> are the same, and therefore, the same confinement coefficient  $\alpha$  must be used for both the modes. However, the previous studies did not pay attention to this issue.<sup>[15,16]</sup> The result is the intrinsic spectral profile of the  $A'_1$  and  $E'$  modes in 1L MoS<sub>2</sub> NCs is a Lorentzian-like lineshape even though  $L_D$  is reported to be as small as 1 nm.<sup>[16]</sup> Therefore, it is necessary to investigate Raman spectra of 1L MoS<sub>2</sub> NCs prepared by the ion implantation technique in a wide range of ion-implanted dosage ( $\eta_{ion}$ ).

In this Letter, we report the Raman spectroscopy of two-dimensional NCs of 1L MoS<sub>2</sub> prepared by the ion implantation technique in a wide range of  $\eta_{ion}$ .

\*Supported by the National Natural Science Foundation of China under Grant Nos 11225421, 11474277, 11434010 and 11574305, and the National Young 1000 Talent Plan.

\*\*Corresponding author. Email: phtan@semi.ac.cn

© 2016 Chinese Physical Society and IOP Publishing Ltd

The same  $\alpha$  is used to understand the opposite behavior of the frequency evolution between the  $A'_1$  and  $E'$  modes with  $\eta_{\text{ion}}$  by simulating the spectral profiles of the two modes as functions of  $\alpha$  and  $L_D$ . To properly understand the Raman spectra of 1L MoS<sub>2</sub> NCs, the frequency shift and asymmetrical broadening of Raman modes at  $\Gamma$ , the contribution of phonons near the zone edge and the anisotropy of phonon dispersion curves along  $\Gamma$ - $K$  and  $\Gamma$ - $M$  must be considered together.

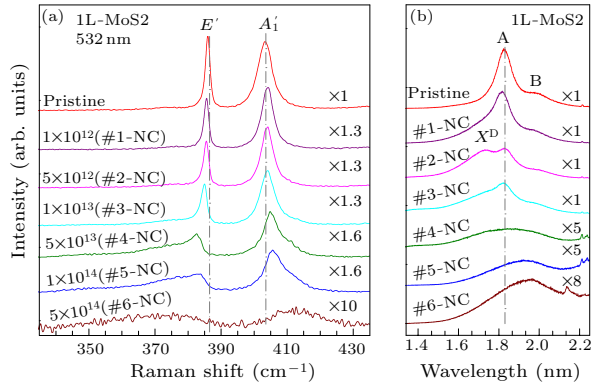


**Fig. 1.** (a) Evolution of the Raman spectra for  $E'$  and  $A'_1$  modes of 1L MoS<sub>2</sub> implanted with different ion dosages. (b) The PL spectra of 1L MoS<sub>2</sub> implanted with different ion dosages. The vertical dashed-dotted lines are guides to the eyes.

The 1L MoS<sub>2</sub> flakes were mechanically exfoliated from bulk crystals. All the flakes were exfoliated onto the Si substrates capped by a 90-nm-thick SiO<sub>2</sub> layer. The layer number was confirmed by ultralow-frequency Raman spectroscopy and photoluminescence (PL) spectra.<sup>[17]</sup> All the optical experiments were carried out in backscattering configuration by using a Jobin-Yvon HR800 system equipped with a liquid nitrogen cooled charge-coupled detector, a  $\times 100$  objective lens and a 1800 line/mm grating. The laser excitation wavelength is 532 nm of a diode-pumped solid-state laser with a power of 50  $\mu$ W to avoid laser heating. Ar<sup>+</sup> implantation is performed to obtain 1L MoS<sub>2</sub> NCs by using an LC-4 type system with a kinetic energy of 100 keV. The samples are subjected to six different  $\eta_{\text{ion}}$  of  $1 \times 10^{12}$ ,  $5 \times 10^{12}$ ,  $1 \times 10^{13}$ ,  $5 \times 10^{13}$ ,  $1 \times 10^{14}$  and  $5 \times 10^{14}$  cm<sup>-2</sup>, and the corresponding samples are denoted as # $n$ -NC,  $n = 1, 2, 3, 4, 5$  and  $6$ , respectively.

Figure 1(a) depicts the Raman spectrum of pristine 1L MoS<sub>2</sub> and those exposed to six different  $\eta_{\text{ion}}$ 's. There are two typical Raman modes,  $E'$  ( $\sim 386.2$  cm<sup>-1</sup>) and  $A'_1$  ( $\sim 404.0$  cm<sup>-1</sup>), in pristine 1L MoS<sub>2</sub>.<sup>[15]</sup> Similar to the case of bulk graphite and few-layer graphenes,<sup>[18,19]</sup> 1L MoS<sub>2</sub> NCs can be formed by the ion-implantation technique. The higher the  $\eta_{\text{ion}}$  is, the smaller the  $L_D$  becomes. The small  $L_D$  of 1L MoS<sub>2</sub> NCs results in frequency shift and asymmetrical broadening of  $E'$  and  $A'_1$  modes. The  $E'$  mode downshifts in frequency and asymmetrical broadening

toward lower frequency, while the  $A'_1$  mode exhibits an opposite behavior with decreasing  $L_D$ , agreeing with the previous works.<sup>[15,16]</sup> In addition, both  $E'$  and  $A'_1$  modes exhibit a decrease in peak intensity, implying that the crystal quality becomes worse and worse with increasing  $\eta_{\text{ion}}$ . This can be further confirmed by the decreased PL intensity of MoS<sub>2</sub> NCs with increasing  $\eta_{\text{ion}}$ , as shown in Fig. 1(b). Some defects and disordered structures are introduced into 1L MoS<sub>2</sub> by the ion implantation, which can trap free charge carriers and localize excitons.<sup>[20,21]</sup> Therefore, a decrease in overall PL intensity of the A exciton is observed with increasing  $\eta_{\text{ion}}$ . However, a new emission peak  $X^D$  ( $\sim 1.74$  eV) is observed below the A exciton ( $\sim 1.83$  eV) in 1L MoS<sub>2</sub> NCs, which can be attributed to the defect-bound neutral excitons.<sup>[20,21]</sup> When  $\eta_{\text{ion}}$  increases up to  $5 \times 10^{13}$  (#4-NC), the PL peak from the A exciton becomes very weak, while the intensity of the  $A'_1$  mode is about half the value in the pristine one. This indicates that the crystal quality of 1L MoS<sub>2</sub> NCs is not so bad even though the corresponding PL emission is almost quenched. It is also found that the PL peak from the A exciton blueshifts with increasing  $\eta_{\text{ion}}$ , as indicated by the vertical dashed-dotted line in Fig. 1(b). This is attributed to the quantum confinement effect of the A exciton in 1L MoS<sub>2</sub> NCs, which has been widely observed in semiconductor quantum wells, wires and dots.<sup>[22]</sup> When  $\eta_{\text{ion}}$  increases up to  $5 \times 10^{14}$  (#6-NC),  $E'$  and  $A'_1$  modes become spectral features with very weak intensity and very broadened profile, indicating that MoS<sub>2</sub> flakes become amorphous.

Before quantitatively analyzing the peak shift and asymmetrical broadening of Raman peaks in 1L MoS<sub>2</sub> NCs, we use the well-known RWL model<sup>[8]</sup> to analyze how the spectral profiles of  $E'$  and  $A'_1$  modes change with the domain size of 1L MoS<sub>2</sub> NCs. Based on the RWL model,<sup>[8]</sup> the lineshape of a Raman mode of general three-dimensional (3D) NCs with a diameter of  $L_D$  is composed of superimposing Lorentzian peaks centered at  $\omega(q)$  and is given by

$$I(\omega) = \int \frac{\exp(-q^2 L_D^2 / 2\alpha)}{(\omega - \omega(q))^2 + (\Gamma_0 / 2)^2} d^3 q, \quad (1)$$

where  $\exp(-q^2 L_D^2 / 2\alpha)$  is a Gaussian-type weighting function describing the participation of phonons away from  $\Gamma$  in the Raman spectra of NCs, the adjustable  $\alpha$  determines how fast the phonon amplitude decays to the NC boundary,  $\Gamma_0$  is the natural broadening, and  $\omega(q)$  is the phonon dispersion curve. In the case of a 3D nanodot,  $d^3 q \propto q^2 dq$ , while for a one-dimensional nanowire with length far larger than diameter,  $d^3 q \propto q dq$ . For 2D NCs with a domain size of  $L_D$ ,  $d^3 q = 2\pi q dq$ . The integral is extended over BZ. Equation (1) shows that the lineshape of the Raman mode is dominated by  $L_D$ ,  $\alpha$  and the corresponding  $\omega(q)$ . Once phonon dispersion curve  $\omega(q)$  of 1L MoS<sub>2</sub>

is determined,<sup>[23]</sup> Eq. (1) can be used to analyze the  $L_D$ -dependent spectral profiles of Raman modes in 1L MoS<sub>2</sub> NCs.

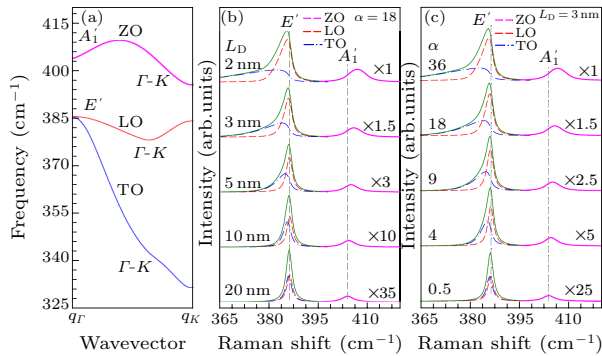


**Fig. 2.** (a) The TO, LO and ZO phonon branches of 1L MoS<sub>2</sub> along  $\Gamma$ -K. (b) Size-dependent  $E'$  and  $A'_1$  line shapes of 1L MoS<sub>2</sub> NCs with  $\alpha$  of 18. (c)  $\alpha$ -dependent  $E'$  and  $A'_1$  line shapes of 1L MoS<sub>2</sub> NCs with  $L_D$  of 3 nm. The dashed-dotted and dashed lines denote the components from TO and LO phonon branches, respectively. The vertical dashed lines are guides to the eyes.

The  $A'_1$  mode is the zone-center mode of the out-of-plane optical (ZO) branch, and the  $E'$  mode is the zone-center mode of in-plane longitudinal optical (LO) and transverse optical (TO) branches, which are experimentally degenerate  $386.2 \text{ cm}^{-1}$  at  $\Gamma$ . The dispersion of ZO, TO and LO branches of 1L MoS<sub>2</sub> along  $\Gamma$ -K is depicted in Fig. 2(a).<sup>[23]</sup> We assume that  $q \neq 0$  phonons in the two branches contribute equally to the broadening of the  $E'$  mode in 1L MoS<sub>2</sub> NCs. Figure 2(b) shows the calculated profiles for  $E'$  and  $A'_1$  modes as a function of  $L_D$  for a fixed  $\alpha$  of 18. The simulated intensity of the  $E'$  mode increases rapidly with decreasing  $L_D$  due to the fact that more and more  $q \neq 0$  phonons are involved in the Raman scattering. Since the decrease trend of the TO branch away from  $\Gamma$  is much faster than the LO branch, the corresponding component (dashed-dotted lines) of the TO branch in the simulated lineshape is much broader than that (dashed lines) of the LO branch. Meanwhile, the TO component exhibits larger red shift of the peak position than the LO branch. Due to the fact that the phonon uncertainty of  $\Delta q$  is mainly determined by  $L_D$  of 2D NCs, the total phonon number involved in the  $E'$  mode of 2D NCs should be the same for the LO and TO branches. Compared with the LO component, the broader line shape for the TO component should result in its low peak intensity. Indeed, in Fig. 2(b), the LO component is much stronger than the TO component in peak intensity. Consequently, the overall line shape of the  $E'$  mode in 2D NCs is mainly dominated by the LO component. For a 2D NC with a fixed  $L_D$ , the  $\alpha$ -dependent lineshape of the  $E'$  mode with increasing  $\alpha$  is depicted in Fig. 2(c), which is very similar to the  $L_D$ -dependent lineshape of the  $E'$  mode with decreasing  $L_D$ . Indeed, since  $\alpha$  demonstrates how fast the phonon amplitude decays to the NC boundary, the

larger the  $\alpha$ , the stronger the confinement effect for the Raman mode.

Based on the above discussion, we now turn to interpret the line shape and peak position of  $E'$  and  $A'_1$  modes of 1L MoS<sub>2</sub> NCs observed in Fig. 1. The same  $\alpha$  must be proposed for both  $E'$  and  $A'_1$  in 1L MoS<sub>2</sub> NCs due to the fact that the phonon uncertainty of  $\Delta q$  is mainly determined by  $L_D$  of 2D NCs. Phonon dispersion of the LO, TO and ZO branches are anisotropic along  $\Gamma$ -K and  $\Gamma$ -M, as shown in Fig. 3(a).<sup>[23]</sup> To minimize this effect on the experimental results, each branch is obtained by averaging the corresponding dispersion curves between high-symmetry directions of  $\Gamma$ -K and  $\Gamma$ -M. Then, the Raman lineshape of  $E'$  and  $A'_1$  modes in 1L MoS<sub>2</sub> NCs can be calculated by Eq. (1). Figure 3(b) depicts the experimental spectra (crosses) of #1-NC and #5-NC and the corresponding theoretical curves (dashed lines). Here  $\alpha = 18$  gives a good fitting to the experimental results and the fitted  $L_D$ 's are 12 nm and 3 nm, respectively, for #1-NC and #5-NC. With decreasing  $L_D$  from 12 nm to 3 nm, the  $E'$  mode exhibits a redshift of  $2.1 \text{ cm}^{-1}$  while the  $A'_1$  mode blue shifts  $1.7 \text{ cm}^{-1}$ . In the fitting, we find that the redshift of the  $E'$  mode is mainly contributed from the TO branch. Indeed, as shown in Fig. 2, if the LO branch is taken into account with the same weight as the TO branch, the LO branch will dominate the lineshape and redshift of small-sized MoS<sub>2</sub> NCs, and the redshift of the  $E'$  mode should be smaller than the blueshift of the experimental profile of the  $A'_1$  mode, which does not coincide with the experimental results.

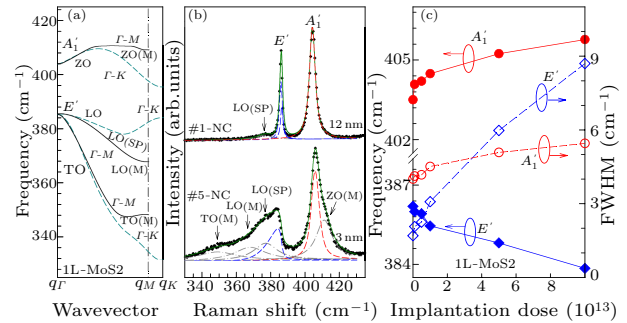


**Fig. 3.** The TO, LO and ZO phonon branches of 1L MoS<sub>2</sub> adopted from Ref. [23]. (b) The experimental (plus sign) and fitted results (green solid lines) of two 1L MoS<sub>2</sub> NCs. The blue and red dashed lines are the fitted  $E'$  and  $A'_1$  curves, respectively, and the grey dashed-dotted lines are Lorentzian fits for defect-induced peaks. (c) Peak position and FWHM of  $E'$  and  $A'_1$  modes dependent on  $\eta_{\text{ion}}$ . Solid and dashed lines are guides to the eyes.

It is noteworthy that when  $\eta_{\text{ion}} > 5 \times 10^{13}$ , the high-energy side of the  $E'$  mode and the low-energy side of the  $A'_1$  mode can be well fitted by the RWL model, however, its asymmetric tail of the  $E'$  mode extends down to about  $330 \text{ cm}^{-1}$ , and that of the  $A'_1$  mode extends up to  $430 \text{ cm}^{-1}$ . As indicated by the gray dashed-dotted lines in Fig. 3(b), four additional modes must be included to obtain a good fit

to the whole profile near  $E'$  and  $A'_1$  modes, which are associated with high phonon density of states near the BZ boundary. They can be activated by the defects-induced selection rule relaxation in the Raman scattering from NCs and are identified as TO(M) at  $\sim 349\text{ cm}^{-1}$ , LO(M) at  $\sim 368\text{ cm}^{-1}$ , LO(SP) at  $\sim 377\text{ cm}^{-1}$  and ZO(M) at  $\sim 410\text{ cm}^{-1}$ , respectively, where LO(SP) is the saddle point (SP) of the LO phonon branch, as indicated in Fig. 3(a). With the increasing  $\eta_{\text{ion}}$ , ZO(M), LO(M), LO(SP) and TO(M) become stronger compared to the intensity of  $E'$  and  $A'_1$  modes. Once these modes are taken into account in the fitting, the Raman spectra of 1L MoS<sub>2</sub> NCs can be well understood by the RWL model. The fitted peak position and full width at half maximum (FWHM) of  $E'$  and  $A'_1$  modes are summarized in Fig. 3(c), where  $E'$  and  $A'_1$  modes show opposite behaviors of peak shift. FWHM of the  $E'$  mode increases more sharply with decreasing the NC size than that of the  $A'_1$  mode. For pristine 1L MoS<sub>2</sub> and these implanted by an  $\eta_{\text{ion}}$  not more than  $1 \times 10^{13}$ ,  $\text{FWHM}(E') < \text{FWHM}(A'_1)$ , while for 1L MoS<sub>2</sub> implanted by  $5 \times 10^{13}$  and  $1 \times 10^{14}$ ,  $\text{FWHM}(E') > \text{FWHM}(A'_1)$ . This obviously results from the steeper dispersion of the TO branch than the ZO branch.

**Table 1.** The domain size ( $L_D$ ) of 1L MoS<sub>2</sub> NCs prepared by ion implantation with different  $\eta_{\text{ion}}$ . The fitted  $\alpha$  is 18.

Dosage	$1 \times 10^{12}$	$5 \times 10^{12}$	$1 \times 10^{13}$	$5 \times 10^{13}$	$1 \times 10^{14}$
$L_D(\text{nm})$	12	10	7	4	3

In conclusion, we have studied the Raman spectra of 1L MoS<sub>2</sub> NCs produced by ion implantation. For a good understanding of the Raman spectra of 1L MoS<sub>2</sub> NCs, contribution of phonons near the zone edge and the frequency shift and asymmetrical broadening of Raman modes at  $\Gamma$  must be considered together, which result from the relaxation of  $q \sim 0$  selection rule by the finite  $L_D$  induced by ion implantation. Due to the fact that the phonon uncertainty of  $\Delta q$  is mainly determined by  $L_D$  of NCs, the same  $\alpha$  must be considered for both  $E'$  and  $A'_1$  modes in 1L MoS<sub>2</sub> NCs. With increasing  $\eta_{\text{ion}}$ , the  $A'_1$  mode of 1L MoS<sub>2</sub> NC blueshifts in frequency and shows asymmetric profiles towards higher frequency regions, which is opposite to the case of the  $E'$  mode. This provides one with a

method to probe the trend of phonon branches away from  $\Gamma$  for other 2D materials.

## References

- [1] Novoselov K S, Geim A K, Morozov S V, Jiang D, Katsnelson M I, Grigorieva I V, Dubonos S V and Firsov A A 2005 *Nature* **438** 197
- [2] Wang Q H, Kalantar Z K, Kis A, Coleman J N and Strano M S 2012 *Nat. Nanotechnol.* **7** 699
- [3] Chhowalla M, Shin H S, Eda G, Li L J, Loh K P and Zhang H 2013 *Nat. Chem.* **5** 263
- [4] Mak K F, Lee C, Hone J, Shan J and Heinz T F 2010 *Phys. Rev. Lett.* **105** 136805
- [5] Yao Z, Kane C L and Dekker C 2000 *Phys. Rev. Lett.* **84** 2941
- [6] Kaasbjerg K, Thygesen K S and Jacobsen K W 2012 *Phys. Rev. B* **85** 115317
- [7] Zeng H L, Dai J F, Yao W, Xiao D and Cui X D 2012 *Nat. Nanotechnol.* **7** 490
- [8] Richter H, Wang Z and Ley L 1981 *Solid State Commun.* **39** 625
- [9] Campbell I and Fauchet P 1986 *Solid State Commun.* **58** 739
- [10] Comas F, Trallero Giner C and Riera R 1989 *Phys. Rev. B* **39** 5907
- [11] Zi J, Zhang K M and Xie X D 1998 *Phys. Rev. B* **58** 6712
- [12] Arora A K, Rajalakshmi M, Ravindran T R and Sivasubramanian V 2007 *J. Raman Spectrosc.* **38** 604
- [13] Gouadec G and Colomban P 2007 *Prog. Cryst. Growth Des. Charact. Mater.* **53** 1
- [14] Adu K, Williams M, Reber M, Jayasingha R, Gutierrez H and Sumanasekera G 2012 *J. Nanotechnol.* **2012** 18
- [15] Zhang X, Qiao X F, Shi W, Wu J B, Jiang D S and Tan P H 2015 *Chem. Soc. Rev.* **44** 2757
- [16] Mignuzzi S, Pollard A J, Bonini N, Brennan B, Gilmore I S, Pimenta M A, Richards D and Roy D 2015 *Phys. Rev. B* **91** 195411
- [17] Qiao X F, Li X L, Zhang X, Shi W, Wu J B, Chen T and Tan P H 2015 *Appl. Phys. Lett.* **106** 223102
- [18] Ferreira E H M, Moutinho M V O, Stavale F, Lucchese M M, Capaz R B, Achete C A and Jorio A 2010 *Phys. Rev. B* **82** 125429
- [19] Li Q Q, Zhang X, Han W P, Lu Y, Shi W, Wu J B and Tan P H 2015 *Carbon* **85** 221
- [20] Chow P K, Gedrim R B J, Gao J, Lu T M, Yu B, Terrones H and Koratkar N 2015 *ACS Nano* **9** 1520
- [21] Tongay S, Suh J, Ataca C, Fan W, Luce A, Kang J S, Liu J, Ko C, Raghunathan R, Zhou J, Ogletree F, Li J, Grossman J C and Wu J 2013 *Sci. Rep.* **3** 2657
- [22] Yu P Y and Cardona M 2005 *Fundamentals of Semiconductors: Physics and Materials Properties* 3rd edn (Berlin: Springer-Verlag)
- [23] Molina-Sánchez A and Wirtz L 2011 *Phys. Rev. B* **84** 155413